



Investigating ultra-low-dose total-body [18F]-FDG PET/CT in colorectal cancer: initial experience

Hui Tan^{1,2,3,4} · Danjie Cai^{1,2,3,4} · Xiuli Sui^{1,2,3,4} · Chi Qi^{1,2,3,4} · Wujian Mao^{1,2,3,4} · Yiqiu Zhang^{1,2,3,4} · Guobing Liu^{1,2,3,4} · Haojun Yu^{1,2,3,4} · Shuguang Chen^{1,2,3,4} · Pengcheng Hu^{1,2,3,4} · Jianying Gu^{4,5} · Hongcheng Shi^{1,2,3,4}

Received: 22 April 2021 / Accepted: 20 August 2021 / Published online: 30 August 2021
© The Author(s), under exclusive licence to Springer-Verlag GmbH Germany, part of Springer Nature 2021

Abstract

Purpose This study was to evaluate the effects of an ultra-low dose of [18F]-FDG on the image quality of total-body PET/CT and its lesion detectability in colorectal cancer (CRC).

Methods Sixty-two CRC patients who underwent total-body PET/CT (uEXPLORER, United Imaging Healthcare, Shanghai, China) with an ultra-low dose (0.37 MBq/kg) of [18F]-FDG were enrolled in this retrospective study. The PET images were reconstructed with the entire 15-min dataset first and then split into 13-, 8-, 5-, 4-, 3-, 2-, and 1-min duration groups to simulate fast scanning images. For simplicity, the images reconstructed with the data from 15 to 1 min were referred to as G15, G13, and so on until G1. Subjective image quality was assessed with 5-point Likert scales. The objective image quality parameters included the SUVmax, SUVmean, and signal-to-noise ratio (SNR) of the liver and blood pool and the SUVmax and tumor-to-background ratio (TBR) of the lesions. G15 served as the control to evaluate lesion detectability.

Results A total of 62 patients (43 men, 19 women; age 41–88, mean \pm SD 64.0 \pm 10.9 years) with 64 CRC primary tumor lesions and 10 low-grade intraepithelial neoplasia (LGIN) lesions were enrolled in this study. The subjective scores were highest for G15 (4.5 \pm 0.5) and then decreased from G13 (4.3 \pm 0.4) to G8 (3.7 \pm 0.5). The liver SNR increased with the extension of acquisition time from G8 (17.2 \pm 2.8) to G13 (20.6 \pm 3.4) and G15 (21.9 \pm 3.4). The liver SNR of G8 was not significantly different from that of G13 ($p=0.15$) and was significantly different from that of G15 ($p=0.001$). All 64 CRC lesions could be identified in all image groups, even on G1. One of ten LGINs was missed on G1, G2, and G3, and one LGIN was missed on G1, G2, G3, and G4. G15 served as the control, and 100% (48/48) lymph nodes could be found on G13 and G8 compared to 93.8% (45/48) lymph nodes on G5 and G4, 85.4% (41/48) lymph nodes on G3, 81.3% (39/48) lymph nodes on G2, and 77.1% (37/48) lymph nodes on G1. For liver metastases, there were no missed liver lesions on G13 and G8 and 3, 4, 6, 7, and 9 missed liver lesions on G5, G4, G3, G2, and G1, respectively. For other areas of metastasis, including the lung, peritoneum, and ovaries, there were no missed lesions in any group.

Conclusions Total-body PET/CT with an ultra-low dose of [18F]-FDG can maintain satisfactory image quality and lesion detectability in CRC.

Keywords Ultra-low dose · Total body · PET/CT imaging · Colorectal cancer

Hui Tan and Danjie Cai equally contributed to this work.

This article is part of the Topical Collection on Oncology—Digestive tract

✉ Hongcheng Shi
shihongcheng163@163.com

¹ Department of Nuclear Medicine, Zhongshan Hospital, Fudan University, 180 Fenglin Road, Shanghai 200032, China

² Nuclear Medicine Institute of Fudan University, Shanghai 200032, China

³ Shanghai Institute of Medical Imaging, Shanghai 200032, China

⁴ Cancer Prevention and Treatment Center, Zhongshan Hospital, Fudan University, Shanghai, China

⁵ Department of Plastic Surgery, Zhongshan Hospital, Fudan University, Shanghai 200032, China

Introduction

Colorectal cancer (CRC) is the second leading cause of cancer death and the third most frequently diagnosed cancer worldwide [1]. Positron emission tomography (PET) integrated with computed tomography (CT) is recommended to assess the resectability of potentially surgically curable CRC according to the NCCN guidelines [2]. The other uses of [18F]-FDG PET/CT in clinical practice for CRC include diagnosing tumors, staging disease, restaging disease, and evaluating treatment efficacy [3–6].

The axial field of view (AFOV) of conventional commercial PET/CT is approximately 15 to 30 cm. This short AFOV restricts the detection efficiency and sensitivity of the system, leading to limited image quality. To acquire whole-body PET images, conventional PET/CT still needs 5 to 9 bed positions to cover the entire torso and legs, which not only reduces the throughput but also limits the patients' cooperation. Total-body PET/CT has been introduced into clinical practice [7, 8]. This system has an AFOV of 194 cm and was reported to have a spatial resolution of 2.9 mm, with time-of-flight (TOF) capability for a time resolution of ~430 ps and energy resolution of 11.7%, according to the NEMA NU-2 2018 protocol [9]. This system provided an ultra-high sensitivity of 174 kcps/MBq and a peak noise-equivalent count rate (NECR) of approximately 2 Mcps for total-body imaging [9].

With these improvements, total-body PET/CT could provide competitive image quality with ultra-low tracer activity. The first human imaging study with total-body PET/CT incorporated an ultra-low dose of injected [18F]-FDG (0.45 MBq/kg), and the images appeared to be of good quality [10]. After that, several relevant studies were undertaken by our center to test the clinical practicability of total-body PET/CT [11–14]. In research on fast scanning with a full dose of activity in oncological patients, our team found that a 1-min acquisition time was adequate for clinical diagnosis compared to a 15-min acquisition time, although the image quality was degraded [11]. Another half-dose study of lung cancer revealed that a 2-min acquisition time achieved comparable image quality to the conventional PET/CT protocol [12]. Our recent research also certified that total-body dynamic PET imaging with ultra-low activity could obtain relevant kinetic metrics of [18F]-FDG and comparable image contrast with full-activity imaging [14].

Based on these previous studies, we used an ultra-low dose (0.37 MBq/kg) of [18F]-FDG with a 7–15-min scan duration as one of the routine protocols in our center. Different cancers have different requirements for PET/CT acquisition time and image reconstruction parameters due to differences in the SUV measurements of lesions and

background tissues. We were curious whether protocols could be optimized for one specific disease. Although conventional PET/CT with [18F]-FDG is useful in the N-staging and M-staging of CRC, its sensitivity for LN metastases of CRC is low, and its sensitivity drops for detecting liver metastases smaller than 10 mm [15, 16]. The improvement of sensitivity provided by the total-body PET/CT equipment can increase the lesion detectability in patient with malignant tumor. There have been no studies on total-body PET/CT with an ultra-low dose of [18F]-FDG in CRC. Therefore, in this study, we explored the boundaries of acquisition time for ultra-low-dose [18F]-FDG imaging in CRC and shared our initial experience, providing reference for follow-up multicenter study about total-body PET/CT with low-dose [18F]-FDG.

Materials and methods

Patients

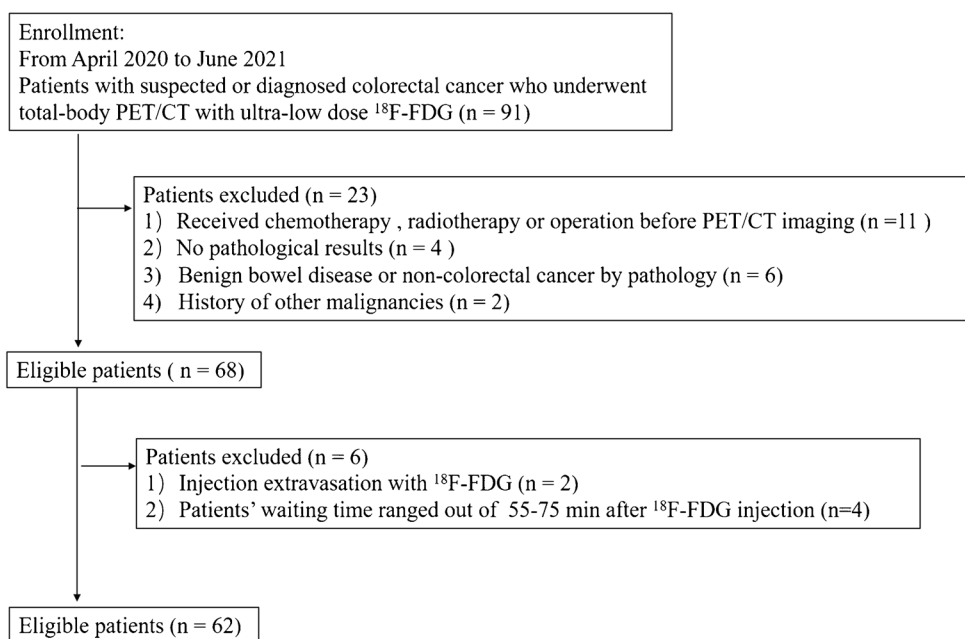
This study was approved by the Medical Ethics Committee of Zhongshan Hospital Affiliated to Fudan University (2019-029R), and informed consent was obtained. From April 2020 to June 2021, a total of 91 consecutive patients with suspected or diagnosed colorectal cancer underwent total-body PET/CT with ultra-low dose (0.37 MBq/kg) were analyzed. The inclusive criteria for this study were as follows: (a) colorectal cancer confirmed with a histologic examination, (b) no previous chemotherapy, radiotherapy, or surgery before PET/CT, and (c) no history of other malignancies. Among the 91 patients, 29 were excluded from this study, as shown in Fig. 1. A total of 62 patients fulfilled all the eligibility criteria.

Total-body PET/CT examination

Patients received a weight-based (0.37 MBq/kg) injection of [18F]-FDG. All patients were required to avoid strenuous exercise within 24 h and fast for at least 6 h before [18F]-FDG imaging. Blood glucose levels were measured at the time of [18F]-FDG injection. Before the [18F]-FDG injection, the fasting blood glucose level need to be less than 11 mmol/L. All patients rested quietly for approximately 60 min post-injection and then underwent PET/CT imaging [17].

3D list-mode PET data were acquired for 15 min on a total-body PET/CT (uEXPLORER, United Imaging Healthcare, Shanghai, China) with a long AFOV of 194 cm. First, the PET images were reconstructed with the entire 15-min dataset, and then the data were split into 13-, 8-, 5-, 4-, 3-, 2-, and 1-min duration groups to simulate fast scanning images. For simplicity, the images reconstructed

Fig. 1 Study flowchart summarizing the patient enrolment process

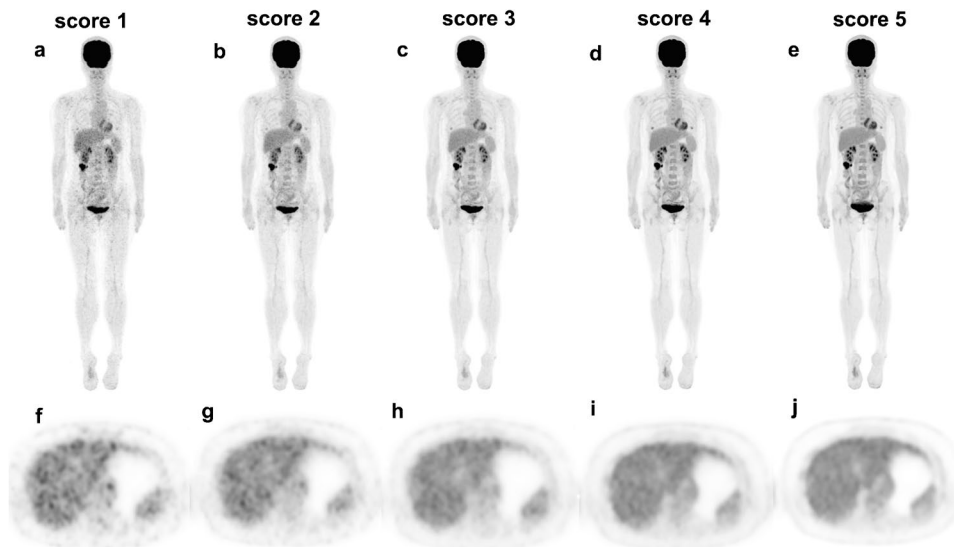


from the 15- to 1-min datasets were referred to as G15, G13, G8, G5, G4, G3, G2, and G1 in the rest of this paper. All PET images were reconstructed with the ordered subset expectation maximization algorithm (OSEM) with the following parameters: TOF and PSF modeling, 2 iterations and 20 subsets, matrix 192×192 , slice thickness 1.443 mm, FOV 600 mm (pixel size $3.125 \times 3.125 \times 2.89 \text{ mm}^3$) with a Gaussian postfilter (3 mm), and all necessary corrections, such as attenuation and scatter correction. The details of the CT scan parameters were as follows: tube voltage 120 kV, tube current 140 mAs, pitch 1.0, collimation 0.5 mm, and reconstructed slice thickness 0.5 mm.

Qualitative PET/CT image analysis

The acquired images were analyzed by two nuclear medicine physicians with 10 years of experience. A vendor-provided workstation (uWS-MI, United Imaging Healthcare) was used to process the data. For accuracy, two readers evaluated the images individually. They assessed subjective image quality with 5-point Likert scales [18]. The scoring criteria were as follows: 1 for very poor image quality, 2 for poor image quality, 3 for average image quality, 4 for good image quality, and 5 for very good image quality. The schematic diagram is shown in Fig. 2. Only images with scores of 3 and higher were defined as qualified to meet the need for clinical

Fig. 2 Schematic diagram of the 5-point Likert scales: score of 1 for very poor image quality, score of 2 for poor image quality, score of 3 for average image quality, score of 4 for good image quality, and score of 5 for very good image quality. The schematic diagram of the 5-point Likert scales is shown on a maximum intensity projection (MIP) (a–e) and corresponding axial image of the liver (f–j)



diagnosis. Images with scores under 3 did not meet the need for clinical diagnosis.

The objective image quality evaluations were performed by an experienced nuclear medicine physician. A 2D circular region of interest (ROI) avoided the vessel walls was placed in the ascending aorta root, which was considered as the blood pool. The maximum standard uptake value (SUV_{max}), mean standard uptake value (SUV_{mean}), and the standard deviation (SD) of the ROI in the blood pool were recorded. The signal-to-noise ratio (SNR) of the blood pool was calculated by dividing the SUV_{mean} by its SD. Four circular 2D ROIs were placed in the following sites in the liver: (1) hepatic dome, (2) right posterior lobe in portal vein layer, (3) left lobe in portal vein layer, and (4) inferior horn of right lobe of liver. The diameters of these four ROIs were 20 mm, and the ROIs avoided intrahepatic lesions and large blood vessels. The SUV_{max}, SUV_{mean}, and SD of the ROIs of the four different liver lesions were recorded, and an average was taken to represent the final SUV_{max}, SUV_{mean}, and SD of the liver. The calculation of the liver SNR was the same as that of the blood pool. To ensure that the size and location of the ROIs were identical for each patient's images, the ROI measurements were made first on G15, and then the copy-and-paste function was used to measure the lesion on G13, G11, G8, and so on down to G1.

Volumes of interest (VOIs) were placed on lesions in the colorectum, lymph nodes, liver, and metastases to other organs for SUV_{max} measurements. If multiple lesions of the colorectum and lymph nodes were found, all of them were analyzed in this study. All patients with fewer than 10 liver lesions, all of them were analyzed in this study. However, for cases of more than 10 liver lesions, we selected the largest lesion for analysis in this study. The tumor-to-background ratio (TBR) was calculated by dividing the SUV_{max} of the lesions by the SUV_{mean} of the liver. To ensure that the size and location of the VOIs were identical across each patient's images, the VOI measurements were made first on G15, and then the copy-and-paste function was used to measure the lesion on G13, G11, G8, and so on down to G1.

Lesion detectability

In this study, lesion detectability was measured by the lesion detection rate. Two nuclear medicine physicians who assessed the subjective image quality read all PET images in a joint session. The order of the images was randomized to avoid the memory effect. All FDG-avid lesions, including colorectal, lymph node, and liver lesions as well as metastatic lesions in other organs were counted only if they could be confidently identified by the readers. The location of the lesion was recorded. The results of

G15 served as the control to assess lesion detectability in the other groups. Lymph nodes were graded as malignant or benign based on functional criteria on PET/CT, and the metastatic lymph nodes were categorized as positive based on their increased [18F]-FDG uptake relative to the surrounding background, independent of their size. A true positive was defined as a match between the location of the metastatic lymph nodes on pathologic examination and the location of the positive lymph nodes on [18F]-FDG PET/CT imaging.

Statistical analysis

Statistical analyses were performed with SPSS 23.0 software for Windows (IBM SPSS Inc., Armonk, NY, USA), and *p* values < 0.05 were considered significant. The inter-rater agreement of subjective image scores was tested with the weighted kappa test, and a kappa value > 0.81 was considered to indicate excellent agreement. Friedman's test with post hoc comparisons Bonferroni-adjusted for multiple comparisons was used to compare differences in the subjective image quality score and lesion SUVs among groups.

Results

Patient characteristics

A total of 62 patients (43 men and 19 women) were enrolled in this study, with an average age of 64.0 ± 10.9 years and body mass index (BMI) of 23.8 ± 3.4 kg/m². The injected FDG dose was 25.3 ± 4.8 MBq. The average blood glucose level before injection was 5.8 ± 1.0 mmol/L. The details are listed in Table 1.

There were 51 patients who underwent colorectal cancer surgery performed by experienced colorectal surgeons, and at least 12 LNs were harvested. The diagnoses of the remaining 11 patients were pathologically confirmed through colonoscopy. All 51 patients were pathologically staged according to the 8th American Joint Committee on Cancer (AJCC) staging system. Liver surgery was performed in 3 out of 62 patients. In total, 62 patients had a total of 64 colorectal cancer lesions and 10 low-grade intraepithelial neoplasia (LGIN) lesions certified by pathology. Three patients with colorectal adenocarcinoma were diagnosed with two other LGIN lesions. Two patients with colorectal adenocarcinoma were diagnosed with another tubular adenoma with LGIN. One patient had two adenocarcinoma lesions of the transverse colon and colonic hepatic flexure. One patient with two adenocarcinoma

Table 1 Clinicopathological characteristics of the 62 patients who underwent total-body PET/CT with an ultra-low dose of ¹⁸F-FDG

Characteristic	Value
Age (years)	64.0 ± 10.9 (range 41–88)
Sex	
Male	43 (69.4%)
Female	19 (30.6%)
BMI (kg/m ²)	23.8 ± 3.4
Blood glucose before injection (mmol/L)	5.8 ± 1.0
Injected dose (MBq)	25.3 ± 4.8
Waiting time (min)	63.7 ± 6.5
Overall stage	
I	11 (17.7%)
II	16 (25.8%)
III	24 (38.7%)
IV	11 (17.7%)
Clinical T stage	
T1	2 (3.2%)
T2	10 (16.1%)
T3	24 (38.7%)
T4	26 (41.9%)
Clinical N stage	
N0	29 (46.8%)
N1	20 (32.2%)
N2	13 (21.0%)
Clinical M stage	
M0	51 (82.3%)
M1	11 (17.7%)
Primary site of colorectal cancer	
Colon	30 (48.4%)
Rectum	32 (51.6%)
Primary tumor size(mm)	41.1 ± 17.0

lesions in the colonic splenic flexure and sigmoid colon was diagnosed with another two LGIN lesions.

Subjective image quality scores

The inter-reader agreement of subjective image quality was excellent (kappa = 0.875). Table 2 shows the values of the subjective image quality scores. The average subjective score was highest for G15 (4.5 ± 0.5) and then decreased from G13 (4.3 ± 0.4) to G8 (3.7 ± 0.5), G5 (3.2 ± 0.4), G4 (3.0 ± 0.3), G3 (2.3 ± 0.4), G2 (1.8 ± 0.3), and G1 (1.0 ± 0.0). For G5, G8, G13, and G15, all of the image quality scores were equal to or greater than 3 points, thus meeting the needs of clinical diagnosis. The frequency of image quality scores of 4–5 points was higher for G15 than for G8. The average scores for G8 and G15 were 3.7 ± 0.5 and 4.5 ± 0.5, respectively, with a significant difference (p = 0.012).

Table 2 Subjective image quality (number)

Time	Excellent (score 5)		Good (score 4)		Average (score 3)		Poor (score 2)		Very poor (score 1)		Average score
	Reader 1	Reader 2	Reader 1	Reader 2	Reader 1	Reader 2	Reader 1	Reader 2	Reader 1	Reader 2	
G1	0	0	0	0	0	0	0	0	0	0	1.0 ± 0.0
G2	0	0	0	0	0	3	0	0	0	7	1.8 ± 0.3
G3	0	0	0	0	0	15	0	0	0	0	2.3 ± 0.4
G4	0	0	3	0	0	51	4	0	0	0	3.0 ± 0.3
G5	0	0	14	1	0	47	14	0	0	0	3.2 ± 0.4
G8	4	4	35	1	0	15	46	0	0	0	3.7 ± 0.5
G13	16	16	46	18	0	1	43	0	0	0	4.3 ± 0.4
G15	27	27	35	30	0	0	32	0	0	0	4.5 ± 0.5

Objective evaluation of PET/CT image quality

As shown in Table 3, the liver SNR increased with the extension of acquisition time from G1 (7.1 ± 1.2) to G2 (9.8 ± 2.0), G3 (11.6 ± 2.2), G4 (13.1 ± 2.2), G5 (14.6 ± 2.5), G8 (17.2 ± 2.8), G13 (20.6 ± 3.4), and G15 (21.9 ± 3.4). The liver SNR on G8 was not significantly different from that on G13 ($p=0.15$) and was significantly different from that on G15 ($p=0.001$). In addition, the liver SUVmax decreased from G8 (3.1 ± 0.5) to G13 (3.0 ± 0.5) and G15 (3.0 ± 0.5), with a significant difference between G8 and G13 ($p=0.03$). All the liver SUVmean measurements on G8, G13, and G15 were 2.7 ± 0.5 , with no significant difference between G8 and G13 ($p=0.19$) or between G13 and G15 ($p=0.25$). The SNRs of the blood pool on G8 and G15 were 18.1 ± 4.8 and 21.9 ± 5.6 , respectively, with no significant difference ($p=0.22$). The SUVmax of the blood pool on G8 and G15 were 2.2 ± 0.4 and 2.1 ± 0.4 , respectively, which was a significant difference ($p=0.015$). The SUVmean of the blood pool on G8 (2.0 ± 0.4) was higher than that on G15 (1.9 ± 0.4), with $p < 0.05$. The details are listed in Table 3.

Image analysis of the lesions

Table 4 shows the SUVmax of the colorectal lesions on G1 (21.1 ± 12.6), G2 (24.0 ± 13.8), G3 (25.1 ± 14.2), G4 (25.3 ± 14.1), G5 (24.9 ± 13.8), G8 (24.5 ± 13.1), G13 (24.1 ± 12.8), and G15 (24.0 ± 12.9), with no significant

difference between G8 and G15 ($p=1.00$). The TBRs of the colorectal lesions on G8 (9.2 ± 4.9) and G15 (9.1 ± 4.9) were not significantly different ($p=1.00$). The SUVmax and TBR of lymph nodes were not significantly different between G8 (8.4 ± 6.7 and 3.3 ± 2.5 , respectively) and G15 (8.6 ± 6.7 and 3.5 ± 2.5 , respectively), with $p=1.00$ and $p=0.32$. The SUVmax and TBR of liver lesions were not significantly different between G8 (8.4 ± 4.8 and 3.6 ± 2.4 , respectively) and G15 (8.7 ± 4.7 and 3.8 ± 2.4 , respectively), with $p=1.00$ for both. Other areas with metastasis included the lung, peritoneum and ovaries in this study. The SUVmax and TBR of other lesions were not significantly different between G8 (8.4 ± 5.9 and 3.5 ± 2.4 , respectively) and G15 (8.7 ± 6.2 and 3.7 ± 2.6 , respectively), with $p=1.00$ for both. The details are listed in Table 4.

Lesion detectability

The results of G15 served as the control to assess lesion detectability in the other groups. In the 74 colorectal lesions (10 LGIN lesions, 64 CRC lesions), all 64 CRC lesions could be identified on all images, even G1. One of ten LGIN lesions was missed on G1, G2, and G3 and could be identified on G4, G5, G8, G13, and G15, and one of ten LGIN lesions was missed on G1, G2, G3, and G4 and could be identified on G5, G8, G13, and G15. The other eight LGIN lesions were avid on all images, even G1. The images of the patient with missed LGIN lesions are shown in Fig. 3.

Table 3 The objective image quality values (mean and SD)

Group	G1	G2	G3	G4	G5	G8	G13	G15
Blood pool SUVmax	2.7 ± 0.6	2.4 ± 0.6	2.3 ± 0.5	2.3 ± 0.5	2.2 ± 0.5	2.2 ± 0.4	2.1 ± 0.4	2.1 ± 0.4
Blood pool SUVmean	2.0 ± 0.5	2.0 ± 0.4	2.0 ± 0.4	2.0 ± 0.4	2.0 ± 0.4	2.0 ± 0.4	1.9 ± 0.4	1.9 ± 0.4
Blood pool SNR	7.7 ± 2.3	10.6 ± 2.6	12.7 ± 2.7	14.6 ± 3.7	16.0 ± 4.3	18.1 ± 4.8	21.8 ± 5.6	21.9 ± 5.6
Liver SUVmax	3.8 ± 0.7	3.5 ± 0.6	3.3 ± 0.6	3.2 ± 0.6	3.2 ± 0.6	3.1 ± 0.5	3.0 ± 0.5	3.0 ± 0.5
Liver SUVmean	2.8 ± 0.5	2.8 ± 0.5	2.8 ± 0.5	2.7 ± 0.5	2.7 ± 0.5	2.7 ± 0.5	2.7 ± 0.5	2.7 ± 0.5
Liver SNR	7.1 ± 1.2	9.8 ± 2.0	11.6 ± 2.2	13.1 ± 2.2	14.6 ± 2.5	17.2 ± 2.8	20.6 ± 3.4	21.9 ± 3.4

Table 4 The SUVmax and TBR measurements of the lesions (mean and SD)

Measurement	G1	G2	G3	G4	G5	G8	G13	G15
SUVmax of colorectal lesions	21.1 ± 12.6	24.0 ± 13.8	25.1 ± 14.2	25.3 ± 14.1	24.9 ± 13.8	24.5 ± 13.1	24.1 ± 12.8	24.0 ± 12.9
TBR of colorectal lesions	7.7 ± 4.4	8.8 ± 5.0	9.3 ± 5.2	9.4 ± 5.2	9.3 ± 5.1	9.2 ± 4.9	9.1 ± 4.9	9.1 ± 4.9
SUVmax of lymph node lesions	6.4 ± 4.8	6.8 ± 5.8	7.4 ± 6.5	7.8 ± 6.5	8.1 ± 6.6	8.4 ± 6.7	8.5 ± 6.7	8.6 ± 6.7
TBR of lymph node lesions	2.5 ± 1.7	2.6 ± 2.0	2.9 ± 2.4	3.1 ± 2.5	3.2 ± 2.5	3.3 ± 2.5	3.5 ± 2.6	3.5 ± 2.5
SUVmax of liver lesions	7.9 ± 4.4	7.7 ± 4.3	7.9 ± 4.7	8.2 ± 4.8	8.4 ± 4.8	8.4 ± 4.8	8.6 ± 4.7	8.7 ± 4.7
TBR of liver lesions	3.2 ± 2.2	3.3 ± 2.3	3.4 ± 2.4	3.5 ± 2.5	3.6 ± 2.5	3.6 ± 2.4	3.7 ± 2.4	3.8 ± 2.4
SUVmax of other areas of metastasis	6.1 ± 4.6	6.1 ± 4.7	7.0 ± 5.1	7.4 ± 5.5	7.7 ± 5.6	8.4 ± 5.9	8.6 ± 6.2	8.7 ± 6.2
TBR of other areas of metastasis	2.5 ± 1.9	2.5 ± 1.9	2.9 ± 2.1	3.1 ± 2.2	3.2 ± 2.3	3.5 ± 2.4	3.6 ± 2.6	3.7 ± 2.6

TBR, tumor-to-liver background ratio; other areas of metastasis include the lung, peritoneum, and ovaries

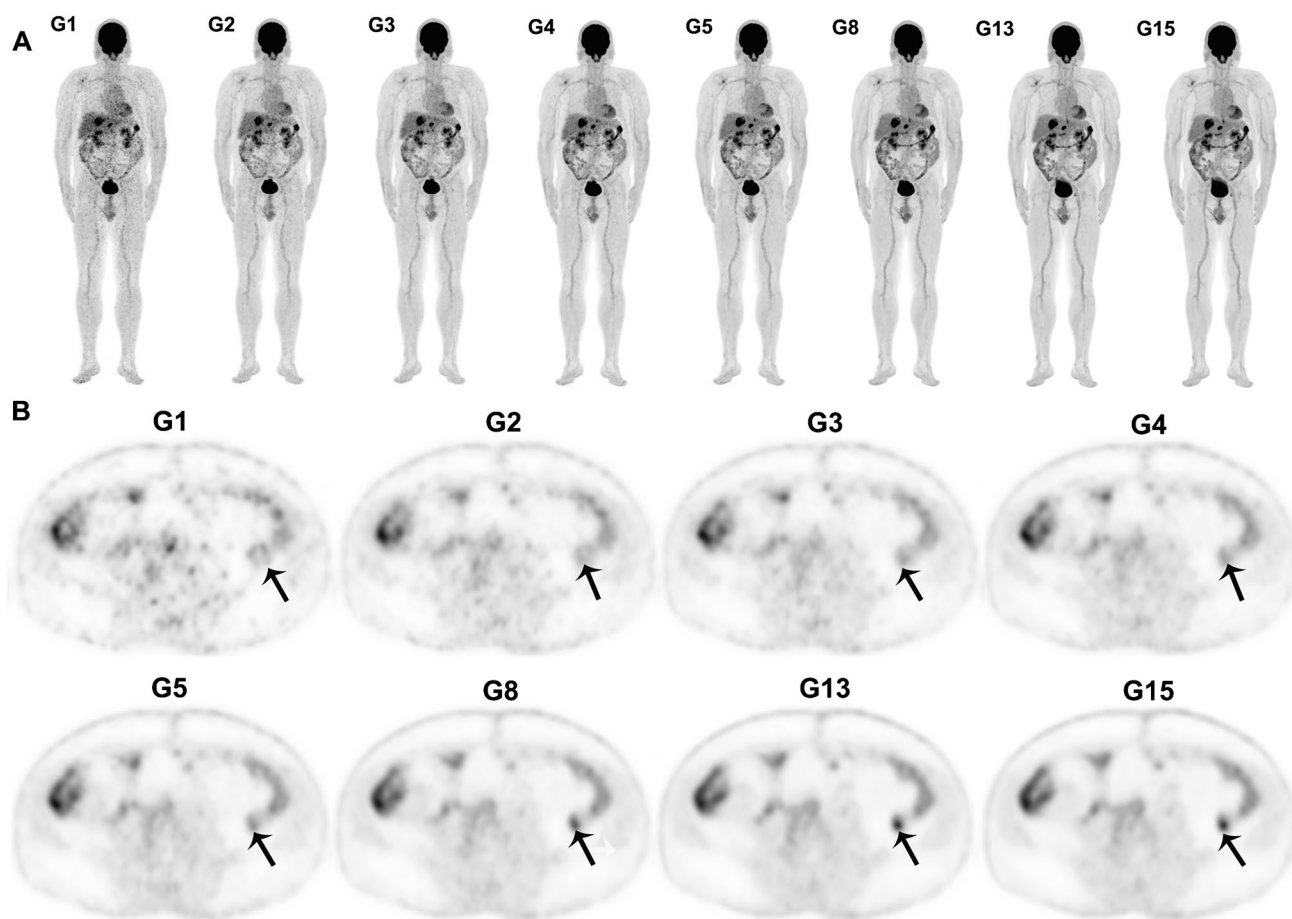


Fig. 3 A 58-year-old male with adenocarcinoma of the splenic flexure of the colon diagnosed with one LGIN lesion and two liver metastases by pathology. No positive peri-intestinal lymph nodes were found after surgery. **(A)** The MIP of the groups with different reconstruction times. The reviewers had the same score, and the subjective image

quality scores were 1 (G1 and G2), 2 (G3), 3 (G4 and G5), 4 (G8 and G13), and 5 (G15). **(B)** The corresponding axial images showed LGIN lesion in colon descendens. The visualization of LGIN lesion was negative on G1, G2, G3, G4, and G5 and positive on G8, G13, and G15

Lymph node metastasis was identified by postoperative pathology in 51 patients. G15 served as the control, on which 48 FDG-positive lymph nodes were identified. On G13 and G8, 100% (48/48) lymph nodes were found, compared to 93.8% (45/48) lymph nodes on G5 and G4, 85.4% (41/48) lymph nodes on G3, 81.3% (39/48) lymph nodes on G2, and 77.1% (37/48) lymph nodes on G1. The short diameters of the missed lymph nodes were less than 9 mm. Four lymph nodes were false positives, which was consistent across groups. A total of 53 lymph nodes turned out to be false negatives, which was consistent across groups. A typical patient with extensive regional lymph node metastasis is shown in Fig. 4.

Liver metastases were identified by PET/CT in 10 of 62 patients. There were 4 patients with more than 10 lesions, 2 patients with 7 lesions, and 2 patients with 2 lesions, and the remaining 2 had one lesion. G15 served as the control, and there were no missed liver lesions on G13 and G8. In

total, 3, 4, 6, 7, and 9 liver lesions were missed on G5, G4, G3, G2, and G1, respectively. The images of a patient with missed liver lesions are shown in Fig. 5. The diameter of all missed liver lesions was less than 15 mm. Metastasis in other areas, including the lung, peritoneum, and ovaries, was identified by PET/CT in 7 of 62 patients. G15 served as the control, and there were no missed lesions in any group.

Discussion

Before the clinical application of total-body PET/CT, the implications brought by a long AFOV and wider acceptance angle were intensively discussed [19]. It was estimated in simulations that gains of up to 40-fold in the effective count rate could be made [20]. Theoretically, an increase in sensitivity could result in a reduction in injected activity and acquisition time in clinical applications [21, 22].

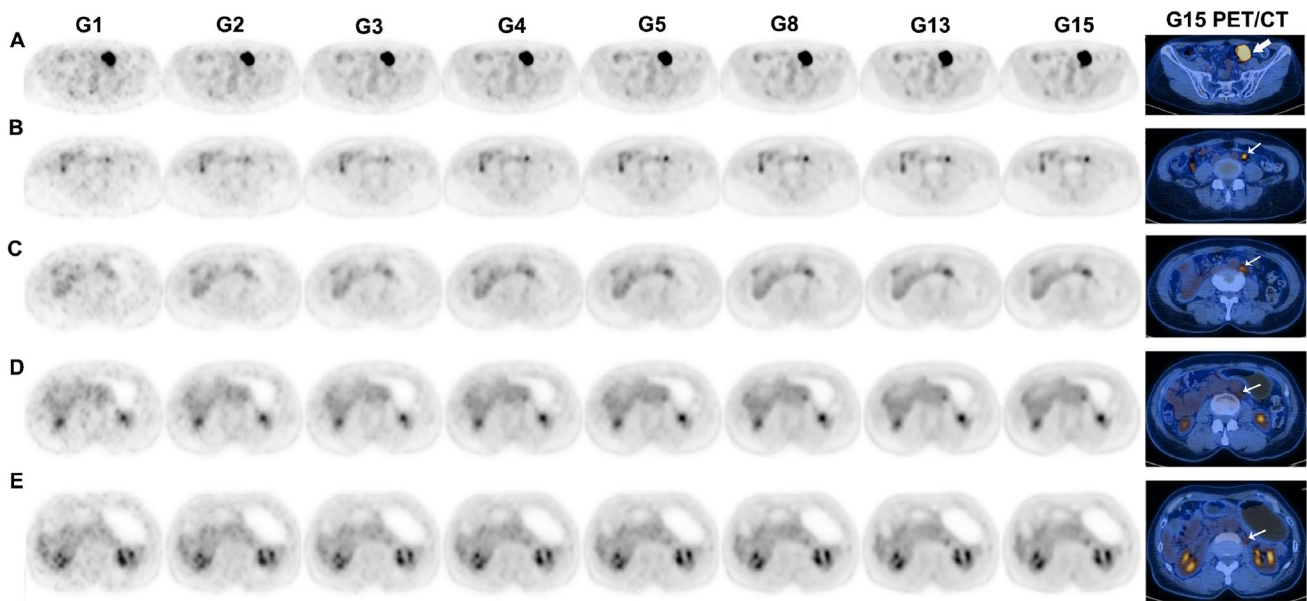


Fig. 4 A 61-year-old female with adenocarcinoma of the sigmoid colon diagnosed by pathology. A total of 13 peri-intestinal lymph nodes were resected, all of which were negative, and one cancerous nodule was found by pathology. The last column shows the 15-min PET/CT fusion images, which showed thickening of the sigmoid colon with abnormal glucose metabolism and enlargement of part of the lymph node next to the left iliac artery and para-aortic region with increased glucose metabolism (shown by the white arrow). (A) The lesion of the sigmoid colon was FDG-avid in each duration group.

(B) The lymph nodes next to the left iliac artery were FDG-avid in each duration group, despite the limited image quality of G1 and G2. (C) The enlarged lymph nodes of the para-aortic region were FDG-negative on G1 and G2 but FDG-avid on G3, G4, G5, G8, G13, and G15. (D) The para-aortic region lymph node was FDG-negative on G1, G2, and G3 but FDG-avid on G4, G5, G8, G13, and G15. (E) The para-aortic region lymph node was FDG-negative on G1, G2, G3, G4, and G5 but FDG-avid on G8, G13, and G15

As mentioned in the “[Introduction](#)” section, our previous research has suggested that ultra-low-dose imaging is possible in clinical practice. In this study on a single disease, we certified the utility of total-body PET imaging with ultra-low [18F]-FDG activity in the clinical diagnosis of colorectal cancer. We attempted to optimize the scanning protocol for one typical disease by reducing the acquisition time and provided our initial experience for the compilation of future clinical guidelines.

The image quality of G8 met the clinical diagnosis needs for CRC without affecting lesion detectability. Regarding subjective image quality scores, G8 (3.7 ± 0.5) had good quality, with all image scores equal to or greater than 3 points. In terms of objective image quality evaluations, the liver SNR of G8 was not significantly different from the liver SNR of G13 ($p=0.15$), but was significantly different from that of G15 ($p=0.001$). G15 served as the control. For colorectal lesions, liver lesions and other metastases were taken into consideration, and all of them could be identified on G8.

The SNR of the liver and blood pool gradually declined from G15 to G1. The shorter the acquisition time, the poorer the PET image quality was, which was consistent with previous studies [23]. This is because the number of measured counts is reduced along with the reduced acquisition time. Additionally, we found that the shortened acquisition time

was accompanied by an increase in both the mean and SD of SUVmax in the liver and the blood pool. In other words, the shortened acquisition time led to deviations in SUVmax caused by noise, as discussed in the research by Halpern et al. [24]. This phenomenon did not occur for the SUVmax of lesions. Therefore, the TBR was not significantly different among G8, G13, and G15 (all $p > 0.05$).

Prior studies found that the specificity of traditional [18F]-FDG PET/CT was relatively high in predicting regional lymph node metastasis in colorectal cancer patients [25–27]. Post-operative inflammation or post-treatment changes were possible reasons for false-positive lymph node findings [28]. In this study, the patients did not receive any treatment before PET/CT imaging. Therefore, the number of false-positive lymph nodes in this total-body PET/CT study was quite small. We observed 4 false-positive lymph nodes, and 1 of them was attributed to peri-intestinal scattering artifacts that occurred in one patient. In this study, a high false-negative rate for lymph nodes was observed with total-body [18F]-FDG PET/CT, similar to in other studies using conventional PET/CT [29]. The high false-negative rate is mainly due to the following reasons. The partial volume effect causes an underestimation of radioactivity concentration for small lymph nodes. For some fused lymph nodes, the number of lymph nodes was underestimated by

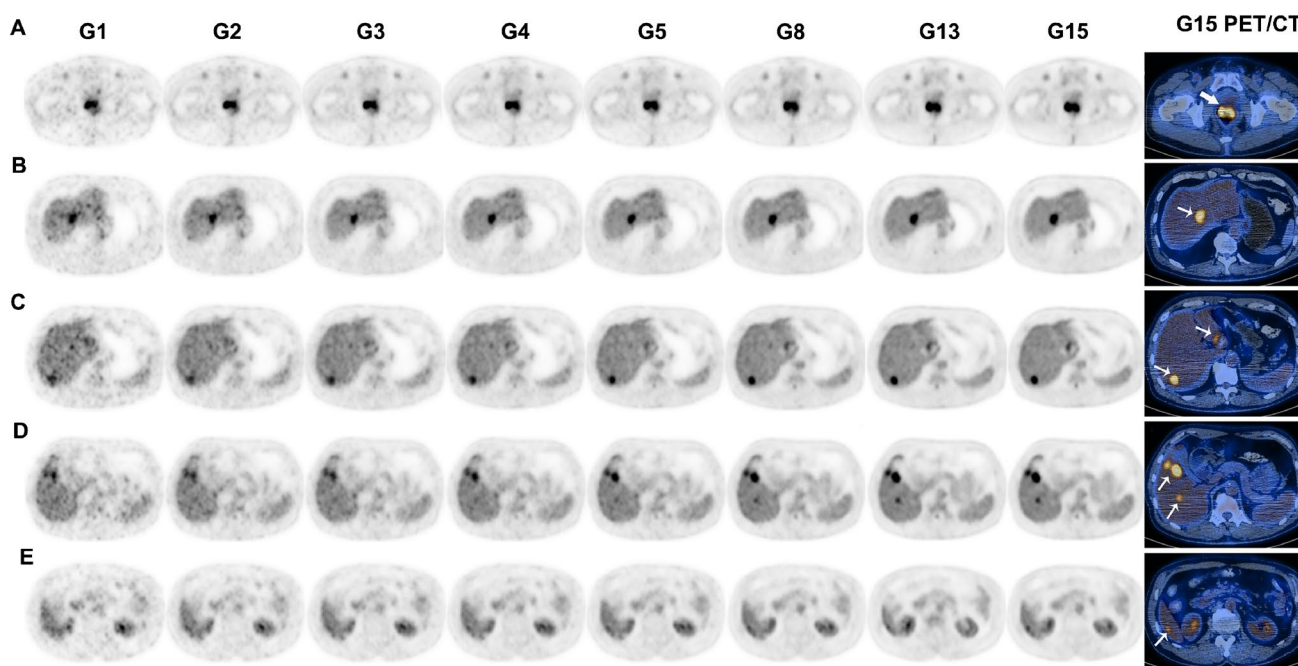


Fig. 5 A 68-year-old male with adenocarcinoma of the rectum diagnosed by pathology of colonoscopy samples. The last column shows the 15-min PET/CT fusion images, which showed thickening and stenosis of the rectum with abnormal glucose metabolism and multiple liver metastases with abnormal glucose metabolism (shown by the white arrow). **(A)** The rectal lesion was FDG-avid in each duration group. **(B, C)** The liver lesions were FDG-avid in each duration

group, despite the limited image quality of G1 and G2. **(D)** The lesion in the right posterior lobe of the liver was FDG-negative on G1, G2, G3, G4, and G5 but FDG-avid on G8, G13, and G15; the remaining two lesions were FDG-avid in each duration group. **(E)** The lesion in the lower corner of the right lobe of the liver was FDG-negative on G1, G2, and G3 but FDG-avid on G4, G5, G8, G13, and G15

PET/CT compared with that by pathology. Metastatic lymph nodes are usually smaller than primary tumors, and adjacent lymph nodes may not be visible as separate structures on PET images.

There were some potential limitations in this study. We excluded patients who were waited time range out of 55–75 min after the [18F]-FDG injection when designing this study. This was because we preferred comparable results that followed that EANM guidelines. However, due to its ultra-high sensitivity, total-body PET/CT could have provided images with good quality even if the waiting time was extended. Nonetheless, further research is needed to reveal the recommended waiting time for total-body PET/CT. In this single-center study, selection bias might exist because of the limited population. Obesity affects PET image quality because of high photon attenuation and scatter. There was no further stratified analysis based on body weight in this study because of the relatively small population. Our study applied the fixed reconstruction method, not the newer generation of PET image reconstruction algorithms such as Bayes penalized reconstruction or deep learning techniques, which will also affect the PET image quality. Our study mainly focused on the analysis of PET

images and not on CT images. In addition, our study was based on FDG injection protocols, and the findings may not be extrapolated to tracers beyond FDG.

With an ultra-high system sensitivity, total-body PET/CT is bound to benefit patients in various fields. Reducing the injected activity and acquisition time was the most meaningful innovation that could benefit patients. This preliminary experience in our center showed that ultra-low-dose [18F]-FDG PET/CT imaging was feasible in the clinical diagnosis and staging of early colorectal cancer. In terms of the PET reconstruction parameters in this study, total-body PET/CT with an ultra-low dose of [18F]-FDG can maintain satisfactory image quality and lesion detectability in CRC. The 8-min acquisition time could meet the clinical needs of colorectal cancer.

Author contribution Hui Tan and Danjie Cai were involved in the study design, data analysis, and manuscript preparation. Xiuli Sui, Chi Qi, Guobing Liu, and Wujian Mao helped with data processing. Haojun Yu and Shuguang Chen helped with image acquisition and processing. Yiqiu Zhang and Pengcheng Hu helped with revision of the manuscript. Jianying Gu and Hongcheng Shi designed the study and contributed to the data analysis and writing of the manuscript. All authors discussed the results and commented on the manuscript.

Funding This study was supported by the National Science Foundation for Scholars of China (No. 81901796), the Shanghai Sailing Program Supported by Shanghai Science and Technology Commission (No. 19YF1408300), Clinical Research Plan of Shanghai Hospital Development Center (No. SHDC2020CR3079B), and the Shanghai Science and Technology Committee (No. 20DZ2201800), Special Fund for Clinical Research, Young Program of Zhongshan Hospital of Fudan University (No. 2018ZSQN38, 2019ZSYQ28, 2020ZSLC63), the Shanghai “Rising Stars of Medical Talent”-Youth Development Program (No. HWJRS2019-720), and the Shanghai Municipal Key Clinical Specialty Project (No. SHSLCZDZK03401). Next Generation Information Infrastructure Construction Project (No. 201901014). Collaborative Innovation Center for Molecular Imaging Precision Medicine, Shanxi Medical University, Taiyuan, Shanxi, 030001, People’s Republic of China.

Data availability The data that support the findings of this study are available from the corresponding author upon reasonable request.

Declarations

Conflict of interest The authors declare no competing interests.

References

- Bray F, Ferlay J, Soerjomataram I, et al. Global cancer statistics 2018: GLOBOCAN estimates of incidence and mortality worldwide for 36 cancers in 185 countries. *CA Cancer J Clin*. 2018;68(6):394–424.
- Benson AB, Venook AP, Al-Hawary MM, et al. Colon cancer, version 2.2021. NCCN clinical practice guidelines in oncology. *J Natl Compr Canc Netw*. 2021;19(3):329–59.
- Rice SR, Chuong M, Koroulakis A, et al. The utility of PET/computed tomography for radiation oncology planning, surveillance, and prognosis prediction of gastrointestinal tumors. *PET Clin*. 2020;15(1):77–87.
- Unterrainer M, Eze C, Ilhan H, et al. Recent advances of PET imaging in clinical radiation oncology. *Radiat Oncol*. 2020;15(1):88.
- Bulens P, Thomas M, Deroose CM, et al. PET imaging in adaptive radiotherapy of gastrointestinal tumors. *Q J Nucl Med Mol Imaging*. 2018;62(4):385–403.
- Rodríguez-Fraile M, Cózar-Santiago MP, Sabaté-Llobera A, et al. FDG PET/CT in colorectal cancer. *Rev Esp Med Nucl Imagen Mol*. 2020;39(1):57–66.
- Zhang X, Xie Z, Berg E, et al. Total-Body dynamic reconstruction and parametric imaging on the uEXPLORER. *J Nucl Med*. 2020;61(2):285–91.
- Zhang X, Cherry SR, Xie Z, et al. Subsecond total-body imaging using ultrasensitive positron emission tomography. *Proc Natl Acad Sci USA*. 2020;117(5):2265–7.
- Spencer BA, Berg E, Schmall JP, et al. Performance evaluation of the uEXPLORER Total-body PET/CT scanner based on NEMA NU 2–2018 with additional tests to characterize long axial field-of-view PET scanners. *J Nucl Med*. 2021;62(6):861–70.
- Badawi RD, Shi H, Hu P, et al. First human imaging studies with the EXPLORER Total-body PET Scanner. *J Nucl Med*. 2019;60(3):299–303.
- Zhang YQ, Hu PC, Wu RZ, et al. The image quality, lesion detectability, and acquisition time of (18)F-FDG total-body PET/CT in oncological patients. *Eur J Nucl Med Mol Imaging*. 2020;47(11):2507–15.
- Tan H, Sui X, Yin H, et al. Total-body PET/CT using half-dose FDG and compared with conventional PET/CT using full-dose FDG in lung cancer. *Eur J Nucl Med Mol Imaging*. 2021;48(6):1966–75.
- Liu G, Xu H, Hu P, et al. Kinetic metrics of (18)F-FDG in normal human organs identified by systematic dynamic total-body positron emission tomography. *Eur J Nucl Med Mol Imaging*. 2021;48(8):2363–72.
- Liu G, Hu P, Yu H, et al. Ultra-low-activity total-body dynamic PET imaging allows equal performance to full-activity PET imaging for investigating kinetic metrics of (18)F-FDG in healthy volunteers. *Eur J Nucl Med Mol Imaging*. 2021;48(8):2373–83.
- Lu YY, Chen JH, Ding HJ, et al. A systematic review and meta-analysis of pretherapeutic lymph node staging of colorectal cancer by 18F-FDG PET or PET/CT. *Nucl Med Commun*. 2012;33(11):1127–33.
- Tsili AC, Alexiou G, Naka C, Argyropoulou MI. Imaging of colorectal cancer liver metastases using contrast-enhanced US, multidetector CT, MRI, and FDG PET/CT: a meta-analysis. *Acta Radiol*. 2021;62(3):302–12.
- Boellaard R, Delgado-Bolton R, Oyen WJ, et al. FDG PET/CT: EANM procedure guidelines for tumour imaging: version 2.0. *Eur J Nucl Med Mol Imaging*. 2015;42(2):328–54.
- Van Sluis J, Boellaard R, Somasundaram A, et al. Image quality and semiquantitative measurements on the biograph vision PET/CT system: initial experiences and comparison with the biograph mCT. *J Nucl Med*. 2020;61(1):129–35.
- Zhang X, Zhou J, Cherry SR, et al. Quantitative image reconstruction for total-body PET imaging using the 2-meter long EXPLORER scanner. *Phys Med Biol*. 2017;62(6):2465–85.
- Cherry SR, Jones T, Karp JS, et al. Total-body PET: maximizing sensitivity to create new opportunities for clinical research and patient care. *J Nucl Med*. 2018;59(1):3–12.
- Tan H, Gu Y, Yu H, et al. Total-Body PET/CT: current applications and future perspectives. *Am J Roentgenol*. 2020;215(2):325–37.
- Pan T, Einstein SA, Kappadath SC, et al. Performance evaluation of the 5-Ring GE Discovery MI PET/CT system using the national electrical manufacturers association NU 2–2012 Standard. *Med Phys*. 2019;46(7):3025–33.
- Akamatsu G, Ishikawa K, Mitsumoto K, et al. Improvement in PET/CT image quality with a combination of point-spread function and time-of-flight in relation to reconstruction parameters. *J Nucl Med*. 2012;53(11):1716–22.
- Halpern BS, Dahlbom M, Quon A, et al. Impact of patient weight and emission scan duration on PET/CT image quality and lesion detectability. *J Nucl Med*. 2004;45(5):797–801.
- Lee JY, Yoon SM, Kim JT, et al. Diagnostic and prognostic value of preoperative (18)F-fluorodeoxyglucose positron emission tomography/computed tomography for colorectal cancer: comparison with conventional computed tomography. *Intest Res*. 2017;15(2):208–14.
- Yang Z, Liu Z. The efficacy of (18)F-FDG PET/CT-based diagnostic model in the diagnosis of colorectal cancer regional lymph node metastasis. *Saudi J Biol Sci*. 2020;27(3):805–11.
- Kantorová I, Lipská L, Bělohávek O, et al. Routine (18)F-FDG PET preoperative staging of colorectal cancer: comparison with conventional staging and its impact on treatment decision making. *J Nucl Med*. 2003;44(11):1784–8.
- Marashdeh WM, Al-Mugbel KM, Alebbini MM, et al. Pitfalls and value of organ specific approach in evaluating indeterminate lesions detected on CT in colorectal cancer by [F18] FDG PET/CT. *Eur J Radiol Open*. 2020;7:100264.
- Kwak JY, Kim JS, Kim HJ, et al. Diagnostic value of FDG-PET/CT for lymph node metastasis of colorectal cancer. *World J Surg*. 2012;36(8):1898–905.

Publisher's note Springer Nature remains neutral with regard to jurisdictional claims in published maps and institutional affiliations.